Bioresource Technology 170 (2014) 248–255

Contents lists available at ScienceDirect

Bioresource Technology

journal homepage: www.elsevier.com/locate/biortech

Specific molecular structure changes and radical evolution during biomass–polyethylene terephthalate co-pyrolysis detected by ^{13}C and ^{1}H solid-state NMR

Kwang-Hyun Ko [a], Veena Sahajwalla [a], Aditya Rawal [b,*]

[a] Centre for Sustainable Materials Research & Technology (SMaRT), School of Materials Science and Engineering, University of New South Wales, Sydney, NSW 2052, Australia
[b] Nuclear Magnetic Resonance Facility, Mark Wainwright Analytical Centre, University of New South Wales, Sydney, NSW 2052, Australia

HIGHLIGHTS

- ^{13}C NMR proved cross-linking reaction between biomass and PET during co-pyrolysis.
- Radical effect on faster thermal degradation PET was studied upon co-pyrolysis.
- ^{1}H NMR revealed evolution of radical as a function of temperature and blend ratio.
- Co-pyrolysis samples showed higher radical density than single pyrolysis samples.

ARTICLE INFO

Article history:
Received 29 April 2014
Received in revised form 28 June 2014
Accepted 30 June 2014
Available online 5 July 2014

Keywords:
Co-pyrolysis
Cross-linking reaction
Radical
^{13}C NMR
^{1}H NMR

ABSTRACT

Co-pyrolysis of biomass with polyethylene terephthalate (PET) was studied as a function of blend ratio and co-pyrolysis temperature by ^{13}C and ^{1}H solid-state nuclear magnetic resonance (NMR). The ^{13}C NMR spectra showed that upon heating to 400 °C in presence of the biomass, the formation of crystallites in PET was completely suppressed and that at higher temperatures there was increased formation and growth of the polycyclic aromatic hydrocarbons (PAHs). This change in the PET degradation behaviour was attributed to the presence of radicals formed in char from biomass. The measurement of the ^{1}H–T_1 relaxation enabled monitoring the changes in the concentrations of radicals formed, as a function of the blend ratios and the co-pyrolysis temperatures. It indicated that the increase in the radical concentrations correlated well with the increased degradation of the PET and growth of PAHs.

1. Introduction

The energy recovery of biomass and plastics through pyrolysis has been extensively highlighted for sustainable development (Skreiberg et al., 2011). The use of biomass as an energy source is ubiquitous, accounting for 13% of worldwide energy consumption (Lal, 2005). However a significant fraction of biomass is landfilled or burnt in the field every year (Sugumaran and Seshadri, 2009), which causes the release of vast quantities CO_2 and methane respectively. Macadamia nut shell and coconut shell, which are high residue crops, are among the major contributors to biomass worldwide (Rodrigues et al., 2008; Stephenson, 2005). Coconut shell and macadamia nut shell thus form a ready resource for utilization into functional materials in ways that can help in reducing pressure on petroleum based products as well as offer the potential for carbon sequestration.

In the case of plastics which currently account for 4% of the world total non-renewable petroleum consumption, more than 50% of the production accounts for short-term applications disposable applications. PET usage stands at about 7% of the thermoplastic demand or approximately 50 million tonnes (Sheldon, 2014; Shen et al., 2009), of which very little is recycled (recycle rate for PET is less than 10% in the USA) (Encinar and González, 2008; Kuczenski and Geyer, 2010; White and Hyde, 2011). Thus there is an urgent need for developing avenues that make recycling waste plastics commercially and environmentally more attractive.

Pyrolysis (heating of the material under inert atmosphere between 300 °C and 1000 °C) is a widely adopted technique for energy conversion of solid materials, such as biomass, plastics, hazardous and medical wastes under a vacuum or inert gas environment for the production of gas, liquid and solid hydrocarbons or other valuable chemical feedstocks. Pyrolysis of biomass such as

* Corresponding author.
E-mail address: a.rawal@unsw.edu.au (A. Rawal).

http://dx.doi.org/10.1016/j.biortech.2014.06.109
0960-8524/

macadamia nut shell (MNS) and coconut shell (CNS), and polymers such as polyethylene terephthalate (PET) brings about significant changes in both chemical and physical properties as compared to the starting material (Ateş et al., 2013). The residual char from the pyrolytic reaction is a highly porous solid carbonaceous material with a high fixed carbon content. This char can have multiple uses, for example as a fuel and alternative carbon source for electrode or activated carbon (ACs) manufacture (González et al., 2009) and for removal of impurities from gaseous and liquid streams (Li et al., 2008; Tam et al., 2001). In particular the biomass- and plastics-based ACs have been shown to yield superior electrochemical properties as compared with those of graphite when heat treated below 1000 °C (Freitas et al., 2001).

The composition and distribution of the pyrolytic product (solid, liquid and gas phase products) relies strongly on the composition of the raw materials (Ateş et al., 2013), the heating rates, maximum reaction temperature and reactant/products residence time (Lin et al., 2009). Co-pyrolysis of biomass with synthetic polymers has been known to alter the thermal degradation behaviour as compared with pure materials and yield different compositions of pyrolytic products. This change in the degradation behaviour and product profile has been attributed to a synergistic effect between the biomass-derived char and the hydrocarbon compounds from the polymer degradation. The formation of radicals on biomass plays an important role for the synergistic enhancement of char formation by affecting other carbon structures in the process of co-pyrolysis (Balat, 2008; Ko et al., 2014). As heat treatment temperature increases (>550 °C), the radicals and the presence of high concentrations of polymerisation sites act to completely carbonise the material. A continuous cross-linking reaction leads to the growth of polycyclic aromatic hydrocarbons (PAHs) by means of intermolecular and intramolecular aromatic condensation (Faravelli et al., 2010).

Despite the importance of pyrolysis process as a means of transforming waste products into potentially high value materials, no significant investigation into the complex reaction mechanisms and molecular transformations has been carried out. To date the primary focus of research in this area has been to understand the influence of operating parameters such as heating rate, particle size and gas conditions in order to maximise tar formation. In particular the synergistic effects to maximize char formation and the variation of the radical concentration during co-pyrolysis have not been systematically studied.

The solid-state NMR technique enables direct analysis of pyrolysis-char chemical structure and the radical species formed. ^{13}C NMR is sensitive to the local environment of the carbon species and correlates the evolution of chemical structure to the pyrolysis temperature. Additionally, paramagnetic radical formation during pyrolysis influences the $^{1}H–T_1$ relaxations, which can therefore be used to probe relative concentrations and distributions of the radical species in the char residue (Barton and Lynch, 1989). Here the structural evolution of the char by hydrogen transfer and cross-linking reactions has been informed by ^{13}C NMR spectroscopy, and changes in the temperature and blending ratio during co-pyrolysis are shown to result in very different concentration and distribution of radicals. These results yield insights into the synergistic effect enhancing char formation as well as the influence of relatively subtle differences in substantially changing the extent of char formation.

2. Methods

2.1. Sample preparation

Two biomass samples (B) which are macadamia nut shell (MNS) and coconut shell (CNS) were ground into a powder using knife milling, and PET was ground using cryomill at 25 Hz for 6 min. After grinding, the MNS and CNS were dried at 60 °C for four days to remove unwanted moisture, and then the samples were physically mixed at a various blending ratios, B_{80}/P_{20}, B_{50}/P_{50} and B_{20}/P_{80}. The weight of sample was fixed at 0.75 g. The samples were heat-treated non-isothermally at a heating rate of 3 °C/min up to three different temperatures, 400 °C, 450 °C and 500 °C under nitrogen atmosphere flowing at the rate of 1 L/min. Maximum heat treatment temperature (HTT) of all samples was strictly limited to 500 °C due to increase in conductivity and the occurrence of a maximum radical concentration in the material (Antal and Grønli, 2003; Freitas et al., 2001). Char samples were prepared with a horizontal furnace which can be encased by a specially designed vacuum bag. At the end of pyrolysis, the samples were moved into the cool zone of the tube furnace and allowed to cool for thirty minutes under flowing nitrogen. Upon cooling, the furnace was encased by the vacuum bag, which was then flushed twice with argon. To collect the as-heat treated char, the vacuum bag was used to suppress the contact of oxygen and moisture with the char. Collecting as-heat treated sample without exposing to oxygen and moisture in normal atmosphere is critical due to alteration of the proton relaxation behaviour by oxygen and moisture (Barton and Lynch, 1989). The sealed furnace was then opened under a positive pressure of argon, the sample taken out from the crucible and manually ground into powder. The samples were packed into 4 mm zirconia MAS rotors with airtight kel-F® caps. All analysis was carried out within 10 min after packing.

2.2. ^{13}C CP-TOSS and ^{1}H solid state NMR experiments

All NMR experiments were carried out using a BRUKER AVANCE III 300 spectrometer operating at ^{1}H NMR frequency of 300 MHz and ^{13}C NMR frequency of 75 MHz at room temperature. All samples were finely ground in the vacuum bag and about 80 mg of each sample was packed into a 4 mm zirconia MAS rotor with a kel-F® caps. The MAS rotors were inserted into a 4 mm H-X double resonance MAS probhead and spun at 8–12 kHz. 90° pulse lengths of 4 μs and 3.5 μs were employed for the ^{13}C and ^{1}H channels respectively. ^{13}C CPMAS experiments were acquired at 8 kHz MAS with a 1 ms cross polarization contact time. The TOSS (Total Suppression of Spinning Sidebands) scheme was implemented before detection of the ^{13}C signal and the Spinal-64 scheme with a field strength of 70 kHz was used for ^{1}H decoupling during detection. The $^{1}H–T_1$ measurements were carried out at 12 kHz MAS with a saturation recovery pulse using fifty periods of 200 μs each to saturate ^{1}H magnetization followed by a variable period for the recovery of the ^{1}H magnetization.

2.3. Calculations

2.3.1. Extracting relaxation constants from ^{1}H NMR for analysing the radical concentration

Generally a single-phase model can be applied to the char $^{1}H–T_1$ relaxation due to structural homogeneity. However the proton relaxation within this single phase is driven either by the radicals present in the system (faster relaxation) or by proton–proton spin diffusion process to sites in the vicinity of the radical species (slower relaxation) (Barton and Lynch, 1989).

Thus for all char samples, the ^{1}H saturation recovery behaviour can be closely fitted by the sum of two exponential factors, as written below;

$$y = M_x/M_o = 1 - A_f(e^{-x/t_1}) - A_s(e^{-x/t_2}) \quad (1)$$

where M_x and M_o are the recovered magnetisation after a recovery time x (preceded by a saturation period of 50×200 μs) and the

equilibrium magnetisation, respectively. t_1 and t_2 are the relaxation time constants for the fast and slow relaxing components (by definition $t_1 < t_2$), while A_f and A_s (by definition, $A_f + A_s = 1$) are the fractions of ^{1}H species with the fast (t_1) and slow (t_2) T_1 relaxation respectively. The use of a bi-exponential fitting instead of a stretched exponential is relevant for systems with a fast spin diffusion constant such as the strongly dipolar coupled systems at moderate MAS speeds (Panich and Furman, 2012). The overall T_1 relaxation behaviour of the samples can be defined using the following equation:

$$T_1^{-1} = A_f/t_1 + A_s/t_2 \quad (2)$$

The parameters $T_1{}^{-1}$ and A_f describe the observed the proton relaxation behaviour of heat treated samples used in this study. The overall relaxation constant $T_1{}^{-1}$ is more reliable than the individual component parameters (A_f and A_s) (Barton and Lynch, 1989). The summary of the ^{1}H–T_1 relaxation constants are tabulated in Tables 1–3.

3. Results and discussion

3.1. Thermal degradation of the neat MNS, CNS and PET

The composition and chemical structure of MNS, CNS and PET has previously been studied in detail (Antal et al., 2000; Maxwell et al., 1998; Preston and Sayer, 1992). The ^{13}C CPMAS spectra of as-received MNS, CNS and PET are shown in Fig. S1(a), (e) and (i) respectively. For MNS and CNS, the spectra represent signals corresponding to three main carbon components in biomass which are hemicellulose (peaks at 20.5 ppm and 172 ppm corresponding to the acetyl group), cellulose (peaks between 50 and 90 ppm predominantly belonging to oxygenated aliphatics from cellulose and some hemicellulose) and the lignin (peaks between 110 and 165 ppm associated with aromatic, substituted aromatic and phenolic carbons) (Bardet et al., 2007; Freitas et al., 2001). However an important distinction between as-received MNS and CNS is that the CNS has a lower fraction of lignin as compared to the MNS. This is evident from the reduced intensity of the lignin peaks in Fig. S1(e) as compared to Fig. S1(a). In comparison to the multicomponent spectrum of MNS and CNS, the ^{13}C NMR spectrum of the raw PET shows a simpler spectrum as expected for a synthetic organic polymer (PET peaks at 163 ppm for the ester carbonyl, 133.5 ppm for the un-protonated aromatic carbon, 130 ppm for the protonated carbon and 61.5 ppm for the aliphatic carbon) (Maxwell et al., 1998; Suebsaeng et al., 1984). The as-received PET also shows signals of the amorphous domains which are visible as broad shoulders at 167 ppm and 64 ppm.

^{13}C CPTOSS spectra of neat MNS, pyrolysed at 400 °C, 450 °C and 500 °C with a heating rate of 3 °C/min are shown in Fig. S1(b)–(d) respectively. At 400 °C, MNS is already significantly degraded. In particular the cellulose and hemicellulose which have relatively less thermal stability are completely degraded. This effect is seen by the complete absence of cellulosic and hemicellulosic peak in Fig. S1(b). This degradation accounts for the major part of the weight loss for temperatures up to 400 °C. On the other hand the signal of the methoxyl group corresponding to the pendant group on aromatic structures in lignin is still observed at 55 ppm, which indicates that while the cross linked structure of the lignin may be degrading, at temperatures of around 400 °C, major reorganisation of the lignin into extensive fused aromatic ring type char structure is yet to occur. In addition, ^{13}C CPTOSS spectra of the MNS pyrolysed at 400 °C (Fig. S1(b)) shows an increase in the signal intensity of the aromatic carbon peaks between 130 ppm and 150 ppm along with the appearance of an aldehyde or ketone signal at 200 ppm. These changes indicate the formation of aromatic structures from the degradation products. It is interesting to note that an identical effect is seen for the case of the as received MNS and CNS pyrolysed at 400 °C (Fig. S1(b) and (f) respectively) with the CNS char being structurally identical to the char from the MNS. Even though the CNS had a lower content of lignin as compared to the MNS, during single pyrolysis of the biomass, the varying fractions of lignin, cellulose and hemicellulose do not seem to significantly influence the structure of the char residue. This can be attributed to the fact that above ca. 350 °C, there is complete degradation of the cellulose and hemicellulose leaving only lignin behind. Since lignin in both CNS and MNS has very nearly identical chemical structure, its pyrolysis into char should yield isostructural char.

The predominant component remaining in the biomass char at 400 °C are the aromatic carbons which originated from the lignin structure and the condensation of the degradation products from cellulose and hemicellulose. The char has aromatic carbon resonances at 126.5 ppm and 147 ppm which correspond to the non-oxygenated and oxygenated (phenolic) aromatic carbons, respectively. Additionally there is a significant signal in the aliphatic resonance between 0 ppm and 40 ppm for the biomass chars at 400 °C which corresponds to the residual low molecular weight tar formed from the degradation of the cellulose and hemicellulose.

There are two path ways to produce char from lignocellulose materials: the primary and the secondary reaction. The primary reaction mechanism involves formation of radicals on the lignin aromatic species followed by intermolecular and intramolecular aromatic condensation, resulting in increasing molecular weight PAHs. During the secondary reaction, the active sites on the surface of the char formed during the primary reaction act as a catalyst to decompose tar into coke in the char layer (Faravelli et al., 2010; Neves et al., 2011; Sharma et al., 2004). There is a clear progress of carbonisation of the biomass with increasing heat treatment temperatures, showing the evolution of aliphatic groups from original lignocellulosic components towards aromatic carbon structure (Bardet et al., 2007; Freitas et al., 2001). At a pyrolysis temperature of 450 °C, the degradation of the aliphatic component of lignin is accelerated as observed by the reduction in intensity of the methoxy peak at 57 ppm in Fig. S1(c) and (g) (for the MNS and CNS respectively). Additionally there is a reduction in the intensity of oxygenated aromatic carbon peak at 147 ppm as well as the aldehyde/ketone signal at 200 ppm. This indicates that there is a progressive depletion of lignin structure leading to char formation with increasing aromatic character at this temperature. As the pyrolysis temperature is increased to 500 °C, the MNS and CNS show identical ^{13}C CPTOSS spectra (Fig. S1(d) and (h) respectively) which are dominated by the aromatic peak at 126.5 ppm. This is

Table 1
The summary of the proton relaxing constants for raw PET, raw MNS and raw CNS. In all cases, A_f and A_s are the fractions of the material with fast and slow ^{1}H–T_1 relaxations respectively.

	Sample	A_f	A_s	t_{1A} (ms)	t_{1B} (ms)	T_1^{-1} (s^{-1})
Unheat treated	PET	1	–	5623 ± 19	–	0.17 ± 0.0005
	MNS	0.13 ± 0.01	0.86 ± 0.01	320 ± 50	2292 ± 55	0.79 ± 0.04
	CNS	0.10 ± 0.02	0.89 ± 0.02	1236 ± 19	4187 ± 564	0.29 ± 0.01

Table 2
The summary of the proton relaxing constants for 100 wt.% of PET, MNS and CNS respectively, heat treated at 3 °C/min.

Sample	Temperature (°C)	A_f	A_s	t_{1A} (ms)	t_{1B} (ms)	T_1^{-1} (s^{-1})
100 wt.% MNS	400	0.28 ± 0.03	0.71 ± 0.03	175 ± 22	1041 ± 49	2.29 ± 0.09
	450	0.61 ± 0.02	0.38 ± 0.02	112 ± 5	421 ± 12	6.34 ± 0.14
	500	0.77 ± 0.04	0.22 ± 0.04	63 ± 7	177 ± 5	12.31 ± 0.99
100 wt.% CNS	400	0.27 ± 0.03	0.72 ± 0.03	295 ± 25	1093 ± 37	1.59 ± 0.02
	450	0.68 ± 0.04	0.31 ± 0.04	151 ± 10	375 ± 10	5.35 ± 0.16
	500	0.75 ± 0.03	0.24 ± 0.03	101 ± 10	198 ± 9	8.63 ± 0.65
100 wt.% PET	400	1	–	8310 ± 210	–	0.12 ± 0.002
	450	1	–	6362 ± 39.7	–	0.157 ± 0.0005
	500	1	–	324 ± 11	–	3.08 ± 0.09

Table 3a
The summary of the proton relaxing constants for MNS–PET blends heat treated at 3 °C/min.

Sample	Temperature (°C)	A_f	A_s	t_{1A} (ms)	t_{1B} (ms)	T_1^{-1} (s^{-1})
M_{80}/P_{20}	400	0.26 ± 0.02	0.73 ± 0.02	257 ± 25	1299 ± 46	1.58 ± 0.05
	450	0.46 ± 0.03	0.53 ± 0.03	152 ± 6	474 ± 15	4.16 ± 0.02
	500	0.82 ± 0.06	0.17 ± 0.06	63 ± 14	187 ± 6	13.9 ± 2.4
M_{50}/P_{50}	400	0.25 ± 0.01	0.74 ± 0.01	313 ± 20	1901 ± 40	1.20 ± 0.03
	450	0.28 ± 0.02	0.71 ± 0.02	190 ± 8	644 ± 6	2.58 ± 0.01
	500	0.85 ± 0.04	0.14 ± 0.04	79 ± 13	228 ± 7	11.4 ± 1.5
M_{20}/P_{80}	400	0.10 ± 0.01	0.89 ± 0.01	931 ± 204	7275 ± 180	0.22 ± 0.01
	450	0.21 ± 0.02	0.78 ± 0.02	781 ± 63	3532 ± 85	0.499 ± 0.007
	500	0.78 ± 0.01	0.21 ± 0.01	131 ± 3	380 ± 2	6.56 ± 0.09

Table 3b
The summary of the proton relaxing constants for CNS–PET blends heat treated at 3 °C/min.

Sample	Temperature (°C)	A_f	A_s	t_{1A} (ms)	t_{1B} (ms)	T_1^{-1} (s^{-1})
C_{80}/P_{20}	400	0.26 ± 0.02	0.72 ± 0.02	438 ± 20	1317 ± 20	1.16 ± 0.01
	450	0.39 ± 0.06	0.6 ± 0.06	214 ± 18	577 ± 29	2.86 ± 0.03
	500	0.84 ± 0.06	0.15 ± 0.06	108 ± 6	303 ± 5	8.27 ± 0.02
C_{50}/P_{50}	400	0.28 ± 0.03	0.71 ± 0.03	1019 ± 65	2738 ± 76	0.53 ± 0.006
	450	0.37 ± 0.03	0.62 ± 0.03	231 ± 25	754 ± 140	2.42 ± 0.2
	500	0.78 ± 0.04	0.21 ± 0.04	136 ± 3	316 ± 28	6.39 ± 0.03
C_{20}/P_{80}	400	0.13 ± 0.007	0.86 ± 0.007	1147 ± 57	5051 ± 37	0.283 ± 0.001
	450	0.37 ± 0.02	0.62 ± 0.02	747 ± 26	2316 ± 50	0.76 ± 0.005
	500	0.76 ± 0.08	0.23 ± 0.08	236 ± 12	660 ± 24	3.60 ± 0.04

because the difference in composition of the components does not affect final chemical structure of char (Bardet et al., 2007).

In the case of PET the ^{13}C NMR shows that there is a difference in the thermal degradation process and the resulting structures as compared with that of the biomass due to the very different chemical structure of the PET. Primary degradation of PET is attributed to initiating breakage of the less thermally stable ester carboxyl bond in the main chain by random scission (Suebsaeng et al., 1984). This is seen clearly by comparing the ^{13}C CPTOSS spectra of the unheated PET to the PET heated to 400 °C (Fig. S1(i) and (j) respectively), which are identical except for the reduction in the relative intensity of the ester carbonyl signal at 163 ppm. With increasing heat treatment temperature up to 450 °C, there is a rapid decrease in the intensity of aliphatic carbon and ester carbonyl signals and the splitting of two aromatic resonances in two well defined peaks is no longer observed as seen in Fig. S1(k). In addition, the complete breakdown of the crystalline domains occurs as seen by the disappearance of the sharp peaks and the appearance of broad lineshapes. When the heat treatment temperature is increased to 500 °C (Fig. S1(l)), the NMR indicates a very different structure for the PET char as compared to the biomass char. There are no peaks observed corresponding to the aliphatic and ester carbonyl peaks, while new peaks arising at near 140 ppm corresponding to quaternary aromatic carbons and a peak at 127 ppm associated with protonated aromatic carbons are observed (Freitas et al., 2001; Suebsaeng et al., 1984). In consequence, the series of reactions results in a highly crosslinked polymer char. Additionally the NMR signal of the PET char at 500 °C is much narrower than that of the biomass char, indicating a more homogeneous chemical structure for the PET char as compared to the biomass char.

The ^{13}C NMR shows a clear progress of carbonisation of the biomasses and the PET with increasing heat treatment temperatures. During pyrolysis, around 95 wt.% of cellulose can be volatilized yielding small amounts of fixed carbon (<5 wt.%) (Lin et al., 2009; Shen et al., 2010; White et al., 2011). This is due to the linear chain structure of cellulose, which undergoes rapid degradation over a very narrow temperature range (300–380 °C). In contrast, lignin consisting of a complex network of cross-linked aromatic molecules, degrades over a wide temperature range (200–900 °C). Therefore as compared to cellulose and hemicellulose, lignin is more difficult to break down into small molecules thereby producing more residual char (Mohan et al., 2006; White et al., 2011). The development of the aromatic char structure in the PET follows a more specific pathway of ester bond degradation and recondensation of the low molecular weight aromatic moieties. The char formation has a large influence on altering the thermal degradation mechanism. This is because the char formation suppresses other

reactions forming the volatile tar and results in reducing the amount of tar available. The thermal degradation of cellulose, as an example, eventually forms volatiles through a series of reactions due to absence of cross-linking sites in the cellulose. Aromatic rings on the other hand, act as building blocks allowing for prolonged residence time of volatile fragments to be stabilised and evolved towards the char. In addition, the elimination of small molecules, and then subsequent dehydrogenation upon pyrolysis results in forming aromatic radicals leading to the growth in PAHs structure (Grand and Wilkie, 2000).

3.2. Thermal degradation of biomass–PET blends

The ^{13}C NMR spectra of the pyrolysed biomass–PET blends show that the predominant structural changes due to the co-pyrolysis occur within the PET fraction of the blends and not the biomass fractions (refer Supplementary Figs. S4 and S5 for the total un-subtracted spectra of the pyrolysed blend samples. Fig. S6(a) and (b) demonstrate that co-pyrolysis primarily affects PET and not the biomass.) This effect can be attributed to the fact that although the PET has a higher degradation temperature than the biomass, it melts at ca. 265 °C (Villain et al., 1994), while the biomass does not melt at all. Due to its molten state above 250 °C, it is expected that the PET fraction comes into closer contact with the biomass fraction potentially wetting its surface, as well as becoming permeable to the early degradation products from the biomass. It is hypothesized that the surface radical species on the biomass char and the radicals from the low molecular weight tar then enhance the degradation of the PET (Khan et al., 2005). On the other hand since the biomass carbonizes before the PET, the PET degradation does not have any observable effect on the structure and degradation of the biomass. The spectroscopic advantage of this specific one way effect is that we can subtract out the contribution of the biomass to the NMR spectrum of the blend sample, using the ^{13}C NMR spectrum of the neat pyrolysed biomass (as shown in Supplementary Fig. S6). This yields the NMR signal of only the PET fraction within the blend which is plotted in Figs. S2 and S3 for the CNS–PET and MNS–PET blends respectively. These spectra show the effect of the co-pyrolysis on the PET as a function of the co-pyrolysis temperature and the blend ratio. In the case of both the CNS–PET and MNS–PET blends, the extent of PET degradation increases with the pyrolysis temperature as expected in a manner similar to that seen in the neat PET material (Fig. S1(i)–(l)). However in the case of the blends there is also increased degradation of the PET with increase in the biomass content of the blend, which is consistent with the influence of the increased concentrations of biomass degradation products on the PET. Thus at the lower temperature (400 °C), the ^{13}C NMR spectrum of the PET in the $C_{20}P_{80}$ and $M_{20}P_{80}$ blend is very similar to that of the neat PET (Compare Figs. S2(g) and S3(g) to Fig. S1(J)). However in the blends with 50 wt.% and 80 wt.% biomass, the PET spectra look very different. Specifically, we no longer observe the sharp crystalline PET domains and there is a reduction in the relative intensity of the protonated aromatic peak at 129 ppm as seen in Figs. S2(a) and S2(d) for the CNS–PET blends and S3(a) and S3(d) for the MNS–PET blends. This indicates that even at the lower temperature, presence of biomass (above 20 wt.%), causes degradation and aromatic condensation of the PET to the extent that it is unable to crystallize.

At elevated temperatures of 450 °C and 500 °C, the effect is much more dramatic. We compare the spectra in Fig. S2(a), (d) and (g), for the specific case the CNS–PET blends heated to 400 °C. The increased level of PET degradation is evidenced by the broadening of the PET aromatic, aliphatic and carbonyl peaks. At increased temperatures of 450 °C, in addition to the peak broadening enhanced reduction in the intensity of the aliphatic and carbonyl peaks is observed with increasing biomass fraction. In particular, for the 80 wt.% biomass blends heated to 450 °C, (Fig. S2(b) for $C_{80}P_{20}$ and Fig. S3(b) for $M_{80}P_{20}$) the carbonyl and aliphatic species have almost completely reacted leaving behind mainly the aromatic species, indicating that the PET has almost completely degraded to form char. Upon further increasing the pyrolysis temperature to 500 °C, there is no significant difference in the PET char structure between the 80 wt.% and 50 wt.% biomass blends, with effectively uniformly broad aromatic peaks observed. The PET char structure in the 20 wt.% blend (Fig. S2(i) and S3(i) for the CNS and MNS blends respectively) however, still resembles that of neat PET char (Fig. S1(i)), which indicates that, at the lower concentrations of biomass, there is insufficient interaction between the PET and primary char.

The ^{13}C NMR spectra of the blends heat treated at 450 °C reveals a broad and intense resonance raised between 130 ppm and 140 ppm indicating the growth of PAHs, which is the result of the radical induced degradation and crosslinking of the PET with the biomass char. The signal intensity of newly formed PAHs decreases with an increase in weight fraction of PET. Since the formation of PAHs is more affected by increase in surface area than degree of aromaticity (Sharma et al., 2004), the growth of PAHs is favoured by PET co-pyrolysed with increasing weight fraction of biomass providing more sites for the PET to cross-link with the char from biomass. It must be highlighted that aromatic carbon is resistant to high temperatures, and a thermally stable system. The currently observed result is very different from the co-pyrolysis of biomass with polyolefinic polymers, such as polyethylene and polypropylene, where only hydrogen interaction occurs and results in high yield of tar (Ko et al., 2014).

3.3. ^{1}H NMR experiments for radical analysis

It has previously been shown that in chars pyrolysed at low temperatures, the effective interaction range (r) of unpaired electrons is small compared to the distance between the unpaired electrons (R) due to their lower concentrations in the char (Barton and Lynch, 1989). As a result, fast ^{1}H–T_1 relaxation occurs for a minority of protons in the immediate vicinity (r) of the unpaired electron, while the bulk of the protons which are at an intermediate distance (d), where $r < d < R$, have a slow T_1 relaxation. As the heat treatment proceeds the concentration of unpaired electrons in the char increases to the point where $r \approx R$. At this stage the bulk of the protons in the char are within the effective interaction range and as a result faster overall T_1 relaxation values are observed at the higher temperatures (Barton and Lynch, 1989). Thus, the ^{1}H–T_1 relaxation measurement acts as a unique indicator to monitor the formation, evolution and stabilization of radical species during pyrolysis.

In the present case of co-pyrolysed biomass and PET, we expect interactions between the components degrading at different temperatures to influence the overall radical formation and stabilization which can be detected by ^{1}H–T_1 measurements.

The ^{1}H–T_1 relaxation data of the neat and co-pyrolysed materials were fitted to a bi-exponential behaviour to account for the multi-component nature of the materials (Tables 1–3). In the case of neat PET, which is structurally homogeneous, the ^{1}H–T_1 relaxation behaviour is fit by a single exponential at all temperatures (Table 2). In comparison the MNS and the CNS, show strong bi-exponential behaviour at all temperatures due to the structurally distinct cellulose and lignin phases in the biomass (Table 2). The bi-exponential fits to the ^{1}H–T_1 relaxation data also yield the fractions of slow (A_s) and fast (A_f) relaxing components with corresponding relaxation times T_{1s} and T_{1f}. In the unheated materials A_s refers to the rigid crystalline cellulose component, while A_f refers to the amorphous and dynamically mobile species. However in the case of chars where the radicals drive the T_1 relaxation, A_s

and A_f refer to the regions with low and high density of radicals respectively. In the case of the neat materials, the relaxation data show that the PET is a particularly rigid polymer with long ^1H–T_1 values of ca. 5 s. In the case of the unheated MNS and CNS, there are slow relaxing and fast relaxing components which correspond to the different site specific dynamics within the material. A general trend observed with the char is that as the pyrolysis temperature increases, the values for the ^1H–T_1 decrease, which is consistent with the development of radical species within the material. Additionally, there is a reduction in the difference between the slower relaxing (higher T_1 values) and faster relaxing (lower T_1 values) components in the char with increasing temperature. This reduction is also consistent with the increase in radical density with increasing temperature. As the concentration of the radicals increases, the average distance between the all the ^1H sites and the radical sites decreases, leading to shorter relaxation times or lower values of the measured T_1.

In order to evaluate the multi-T_1 relaxations in the different materials, it is convenient to use the overall relaxation rate of T_1^{-1} as shown in Eq. (2). A higher value of T_1^{-1} corresponds to a faster T_1 relaxation while a smaller value of T_1^{-1} corresponds to a slower T_1 relaxation. The values of the T_1^{-1} for the different materials and different pyrolysis temperatures are plotted in Fig. 1. In the case of the neat unheated materials, the relaxation studies show that the CNS has a smaller value of T_1^{-1} than the MNS (Fig. 1, filled squares). This is consistent with the structure of the CNS which has more of the slow relaxing crystalline cellulose and less of the fast relaxing lignin as compared to the MNS (Antal et al., 2000). In the untreated materials, the presence of the PET, which has the same order of magnitude T_1 relaxation as the biomass, does not significantly alter the overall relaxation behaviour of the blends. As the blends are heated to higher temperatures, we see significant differences between the T_1^{-1} of the different blend samples. In the case of neat PET, there is very little difference between in the T_1^{-1} up to 450 °C due to the relatively minimal degradation of PET up to this temperature. Upon heating to 500 °C there is a rapid increase in the T_1^{-1}, which is attributed to the fast degradation and radical formation within the PET. At the other end of the blend spectrum, in pure biomass samples, the MNS char shows higher T_1^{-1} than the CNS char as the temperature increases, with the greatest difference being at 500 °C (12.31 s^{-1} vs. 8.63 s^{-1} for the MNS and CNS respectively). This difference in the relaxation rates for the biomass must be driven by the difference in the lignin content of these materials which is the primary source of the stable free radical generation within the char.

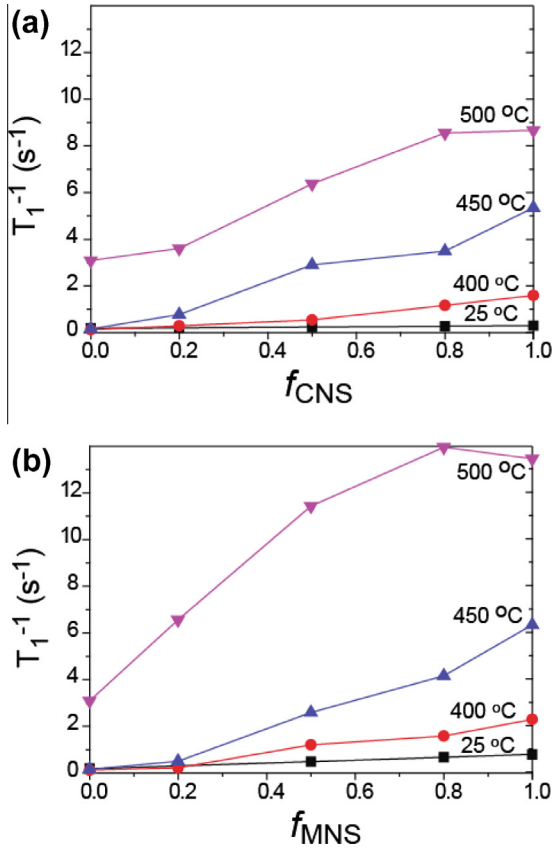

Fig. 1. Plot of the overall ^1H–T_1 relaxation rate of (a) the CNS–PET blends and (b) the MNS–PET blends upon pyrolysis at 400 °C, 450 °C and 500 °C. Filled squares are the relaxation rates for non pyrolysed room temperature (25 °C) raw materials. Filled circles, triangles and inverted triangles are the relaxation rates of blends pyrolysed to 400 °C, 450 °C and 500 °C respectively. Lines are guides to the eye.

It has been known that radicals in lignin tend to propagate and then stabilize themselves via hydrogen abstraction reactions (Faravelli et al., 2010). Textural characteristics (porosity) of chars can also vary with the rate of thermal degradation rate depending on the component composition of the starting materials. Higher hemicellulose and cellulose fractions lead to highly constricted char with a high portion of microporosity (González et al., 2009). The texture characteristic of char plays a primary role in forming polycyclic aromatic hydrocarbons (PAHs) (Sharma et al., 2004). Therefore, differences in radical concentration and behaviour of radical evolution are expected from different types of biomass.

In the case of the copyrolysed blends, a systematic increase in the T_1^{-1} values with increasing temperature is observed, which follows the trend seen in the biomass char, with the highest T_1^{-1} for the blends containing the most biomass ($M_{80}P_{20}$ and $C_{80}P_{20}$). These measurements indicate that the presence high concentration of biomass induces the formation of greater concentration of free radicals within the char, leading to the observed high T_1^{-1} values. It is important to note that even though the PET char by itself has a significantly lower T_1^{-1} value at 500 °C as compared to the neat biomass char, its presence in the $M_{80}P_{20}$ and $C_{80}P_{20}$ blends does not reduce their overall T_1^{-1} values. This is consistent with the previous ^{13}C NMR observations that the structure of the PET char fraction in the blends is different than that of the neat PET char.

Additionally the sorbate molecule (aromatic hydrocarbon from PET) distribution within the char from the biomass is expected to be influenced by the textural properties of the biomass char and can also have a strong influence on radical stabilization. Thus, in the case of the MNS blends, which is expected to have a higher surface area and lower microporosity than the CNS blends, the sorbate molecules have a better interaction with the char surface thereby enhancing the stability of the radical species which leads to higher T_1^{-1} values. Thus the increase in concentration of radicals in biomass and PET derived chars leads to difference in spin–lattice relaxation rates of the chars over various heat treatment temperatures at a specific heating rate.

It is observed in Fig. 1 that the blends have increased value of T_1^{-1} with increasing fraction of biomass. At the higher weight fraction, i.e. 80 wt.% biomass, the blend char has equal if not higher T_1^{-1} that the neat biomass char. This is particularly evident at 500 °C in Fig. 1. This enhanced relaxation behaviour suggests that there is a synergystic effect originating from the 20 wt.% PET in the blend sample. The presence of a synergistic effect enhancing the T_1 relaxation process can observed by comparing the T_1 relaxation expected for a mixture of PET and biomass chars, where there is no interaction, to the T_1 relaxation observed for the actual co-pyrolysed blend samples.

Fig. 2 shows the T_1 relaxation data from the ^1H saturation recovery experiments for $C_{80}P_{20}$ and $M_{80}P_{20}$ blends at different temperatures. The saturation recovery data is well fitted by bi-exponential

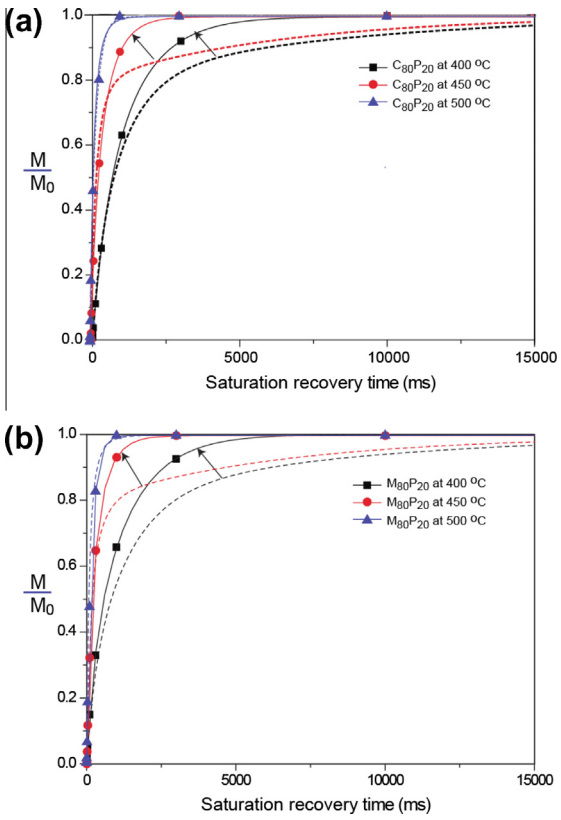

Fig. 2. ^{1}H spin lattice relaxation of (a) $C_{80}P_{20}$ and (b) $M_{80}P_{20}$ blends co-pyrolysed to 400 °C (black squares), 450 °C (red circles) and 500 °C (blue triangles) at a heating rate of 3 °C/min. Solid lines indicate the bi-exponential fits to the data. Dashed lines indicate the simulated behaviour of a 80:20 wt.% mixture of CNS or MNS with PET after separate pyrolysis. Arrows indicate the enhanced relaxation of the blends as compared to the mixtures. (For interpretation of the references to colour in this figure legend, the reader is referred to the web version of this article.)

curves (represented by solid lines), which is consistent with our two domain model for the distribution of the radicals. As expected, the chars have a faster saturation recovery (shorter T_1 or larger T_1^{-1}) with increasing temperature due to the increase in the radical concentration. The dashed lines in Fig. 2 represents the simulated T_1 saturation recovery behaviour of a 80:20 mixture of biomass and PET chars separately pyrolysed at the different temperatures. At the lower temperatures (400 °C and 450 °C), the simulated T_1 saturation recovery is slower than that of the actual co-pyrolysed blends. This indicates that the co-pyrolysed blends have a higher free radical concentration than a similar amount of separately pyrolysed biomass and PET. This enhancement in the free radical concentration must be derived from the chemical interactions between the biomass and the PET, namely hydrogen transfer from the PET to the radicals in the primary char from the biomass. This interaction implies that the biomass char in the blends, accelerates the PET degradation and promotes its conversion to char while the hydrogen transfer from the PET to the biomass char stabilized the radicals. At higher temperature (500 °C), the T_1 saturation recovery of the co-pyrolysed blend and the simulated curves overlap, indicating that there are similar concentrations of free radicals in the separately-pyrolysed materials and co-pyrolysed blends. This is consistent with the fact that the neat PET undergoes relatively slow degradation and has low radical concentration up to 450 °C, (as seen in Fig. 1), but very rapid degradation and char formation at 500 °C which is accompanied with high degree of radical formation (and concomitantly a high value of T_1^{-1}). Thus at the higher temperature, we expect similar concentrations of free radicals in both the separately pyrolysed and co-pyrolysed materials. This radical concentration enhancement at lower temperatures, indicates that the synergistic interactions between the biomass and the PET are most predominant at the lower pyrolysis temperatures.

4. Conclusion

Biomass–PET co-pyrolysis increased the yield of char at reduced temperatures. This increase was due to enhanced PET degradation in blends as compared to neat PET. The enhancement was a result of the interactions of the radicals from the biomass-primary char during co-pyrolysis. The PET–biomass interaction stabilized the radicals in the char thereby increasing the radical concentration and PET degradation at lower temperatures. The radical concentration in the char the PET degradation rate could be controlled by via temperature and blending ratio. Optimal conditions for char formation were found for biomass – 80 wt.% and PET – 20 wt.% blends.

Appendix A. Supplementary data

Supplementary data associated with this article can be found, in the online version, at http://dx.doi.org/10.1016/j.biortech.2014.06.109.

References

Antal, M.J., Allen, S.G., Dai, X., Shimizu, B., Tam, M.S., Grønli, M., 2000. Attainment of the theoretical yield of carbon from biomass. Ind. Eng. Chem. Res. 39 (11), 4024–4031.
Antal, M.J., Grønli, M., 2003. The art, science, and technology of charcoal production. Ind. Eng. Chem. Res. 42 (8), 1619–1640.
Ateş, F., Miskolczi, N., Borsodi, N., 2013. Comparision of real waste (MSW and MPW) pyrolysis in batch reactor over different catalysts. Part I: product yields, gas and pyrolysis oil properties. Bioresour. Technol. 133, 443–454.
Balat, M., 2008. Mechanisms of thermochemical biomass conversion processes. Part 1: reactions of pyrolysis. Energy Sources Part A 30 (7), 620–635.
Bardet, M., Hediger, S., Gerbaud, G., Gambarelli, S., Jacquot, J.F., Foray, M.F., Gadelle, A., 2007. Investigation with 13C NMR, EPR and magnetic susceptibility measurements of char residues obtained by pyrolysis of biomass. Fuel 86 (12–13), 1966–1976.
Barton, W.A., Lynch, L.J., 1989. Proton NMR spin–lattice relaxation in bituminous coals. Energy Fuels 3 (3), 402–411.
Encinar, J.M., González, J.F., 2008. Pyrolysis of synthetic polymers and plastic wastes. Kinetic study. Fuel Process. Technol. 89 (7), 678–686.
Faravelli, T., Frassoldati, A., Migliavacca, G., Ranzi, E., 2010. Detailed kinetic modeling of the thermal degradation of lignins. Biomass Bioenergy 34 (3), 290–301.
Freitas, J.C.C., Bonagamba, T.J., Emmerich, F.G., 2001. Investigation of biomass- and polymer-based carbon materials using 13C high-resolution solid-state NMR. Carbon 39 (4), 535–545.
González, J., Román, S., Encinar, J., Martínez, G., 2009. Pyrolysis of various biomass residues and char utilization for the production of activated carbons. J. Anal. Appl. Pyrol. 85 (1), 134–141.
Grand, A.F., Wilkie, C.A., 2000. Fire Retardancy of Polymeric Materials. CRC Press.
Khan, R., Chu, J., Margrave, J., Hauge, R., Smalley, R., 2005. Free radical chemistry during slow pyrolysis of solid fuels. Energy Sources 27 (3), 279–298.
Ko, K.-H., Rawal, A., Sahajwalla, V., 2014. Analysis of thermal degradation kinetics and carbon structure changes of co-pyrolysis between macadamia nut shell and PET using thermogravimetric analysis and 13C solid state nuclear magnetic resonance. Energy Convers. Manage. 86, 154–164.
Kuczenski, B., Geyer, R., 2010. Material flow analysis of polyethylene terephthalate in the US, 1996–2007. Resour. Conserv. Recycl. 54 (12), 1161–1169.
Lal, R., 2005. World crop residues production and implications of its use as a biofuel. Environ. Int. 31 (4), 575–584.
Li, W., Yang, K., Peng, J., Zhang, L., Guo, S., Xia, H., 2008. Effects of carbonization temperatures on characteristics of porosity in coconut shell chars and activated carbons derived from carbonized coconut shell chars. Ind. Crops Prod. 28 (2), 190–198.
Lin, Y.-C., Cho, J., Tompsett, G.A., Westmoreland, P.R., Huber, G.W., 2009. Kinetics and mechanism of cellulose pyrolysis. J. Phys. Chem. C 113 (46), 20097–20107.
Maxwell, A.S., Ward, I.M., Lauprêtre, F., Monnerie, L., 1998. Secondary relaxation processes in polyethylene terephthalate-additive blends: 1. N.m.r. investigation. Polymer 39 (26), 6835–6849.
Mohan, D., Pittman, C.U., Steele, P.H., 2006. Pyrolysis of wood/biomass for bio-oil: a critical review. Energy Fuels 20 (3), 848–889.
Neves, D., Thunman, H., Matos, A., Tarelho, L., Gómez-Barea, A., 2011. Characterization and prediction of biomass pyrolysis products. Prog. Energy Combust. Sci. 37 (5), 611–630.

Panich, A.M., Furman, G.B., 2012. Nuclear spin–lattice relaxation and paramagnetic defects in carbon nanomaterials. Diam. Relat. Mater. 23, 157–161.
Preston, C.M., Sayer, B.G., 1992. What's in a nutshell: an investigation of structure by carbon-13 cross-polarization magic-angle spinning nuclear magnetic resonance spectroscopy. J. Agric. Food Chem. 40 (2), 206–210.
Rodrigues, S., Pinto, G.A.S., Fernandes, F.A.N., 2008. Optimization of ultrasound extraction of phenolic compounds from coconut (*Cocos nucifera*) shell powder by response surface methodology. Ultrason. Sonochem. 15 (1), 95–100.
Sharma, R.K., Wooten, J.B., Baliga, V.L., Lin, X., Geoffrey Chan, W., Hajaligol, M.R., 2004. Characterization of chars from pyrolysis of lignin. Fuel 83 (11–12), 1469–1482.
Sheldon, R.A., 2014. Green and sustainable manufacture of chemicals from biomass: state of the art. Green Chem. 16 (3), 950–963.
Shen, D., Gu, S., Bridgwater, A., 2010. The thermal performance of the polysaccharides extracted from hardwood: cellulose and hemicellulose. Carbohydr. Polym. 82 (1), 39–45.
Shen, L., Haufe, J., Patel, M.K., 2009. Product overview and market projection of emerging bio-based plastics PRO-BIP 2009. Utrecht University.
Skreiberg, A., Skreiberg, Ø., Sandquist, J., Sørum, L., 2011. TGA and macro-TGA characterisation of biomass fuels and fuel mixtures. Fuel 90 (6), 2182–2197.
Stephenson, R., 2005. Macadamia: domestication and commercialisation. Chron. Horticult. 45 (2), 11–15.
Suebsaeng, T., Wilkie, C.A., Burger, V.T., Carter, J., Brown, C.E., 1984. Solid products from thermal decomposition of polyethylene terephthalate: Investigation by CP/MAS 13C-NMR and Fourier transform-IR spectroscopy. J. Polym. Sci. A: Polym. Chem. Ed. 22 (4), 945–957.
Sugumaran, P., Seshadri, S., 2009. Evaluation of selected biomass for charcoal production. J. Sci. Ind. Res. 68, 719–723.
Tam, M.S., Antal, M.J., Jakab, E., Várhegyi, G., 2001. Activated carbon from macadamia nut shell by air oxidation in boiling water. Ind. Eng. Chem. Res. 40 (2), 578–588.
Villain, F., Coudane, J., Vert, M., 1994. Thermal degradation of poly (ethylene terephthalate) and the estimation of volatile degradation products. Polym. Degrad. Stab. 43 (3), 431–440.
White, J.E., Catallo, W.J., Legendre, B.L., 2011. Biomass pyrolysis kinetics: a comparative critical review with relevant agricultural residue case studies. J. Anal. Appl. Pyrol. 91 (1), 1–33.
White, K.M., Hyde, M.K., 2011. The role of self-perceptions in the prediction of household recycling behavior in Australia. Environ. Behav..